Journal Pre-proof

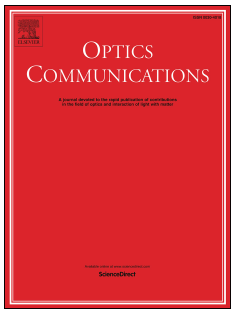

All-optical erasing of photorefractive solitonic X-Junctions in lithium niobate thin-film on insulator

Alessandro Bile, Mathieu Chauvet, Eugenio Fazio

PII: S0030-4018(26)00744-3

DOI: https://doi.org/10.1016/j.optcom.2026.133605

Reference: OPTICS 133605

To appear in: *Optics Communications*

Received Date: 1 April 2026

Revised Date: 17 July 2026

Accepted Date: 20 July 2026

Please cite this article as: A. Bile, M. Chauvet, E. Fazio, All-optical erasing of photorefractive solitonic X-Junctions in lithium niobate thin-film on insulator, *Optics Communications*, https://doi.org/10.1016/j.optcom.2026.133605.

All-optical erasing of photorefractive solitonic X-Junctions in lithium niobate thin-film on insulator

Alessandro Bile,[1,*] Mathieu Chauvet,[2] Eugenio Fazio[1]

[1] Department of Fundamental and Applied Sciences for Engineering, Sapienza University of Rome, via A. Scarpa 16, Rome, Italy
[2] FEMTO-ST Institute, UMR CNRS 6174, University of Franche-Comté, 15B Avenue des Montboucons, 25000 Besançon, France
**Corresponding author: alessandro.bile@uniroma1.it*

Abstract

We report the in-situ erasing of solitonic channels in lithium niobate thin films on insulator (LNOI). The experiments are performed in 8 µm thick films of congruent undoped LiNbO3 to partially or totally erase X-junction structures. The erasing procedure is based on the local application of a strong photovoltaic field that removes the localized photoexcited charge density redistributing it over the whole crystal.

Keywords: spatial solitons; nonlinear optics; erasing method; neuromorphics

Introduction

Over the last 30 years, photorefractive screening solitons [1-3] have attracted great interest as they can be generated with very low light intensities [4] and therefore with a sufficiently low associated technology. Furthermore, over the years the intense bias electric fields that were necessary to induce local screening fields, and consequently the self-focusing and self-confinement effects, have been effectively replaced by pyroelectric fields [5-6] further simplifying the experimental set-up and further reducing the overall complexity. The technological advantage of soliton waveguides lies in the possibility of creating buried waveguides by exploiting the variations in refractive index induced by the optically-excited electric charges [7]. In order to propagate without diffraction, light tends to create channels of modified refractive index which can also be exploited by other light signals as waveguides, remaining confined within them. Being self-written, soliton waveguides are optimized for confined propagation and therefore they have very low propagation losses, a factor that makes them unique in the technological panorama of integrated optics. Not only that: being generated by the distribution of photoexcited electric charge trapped in the crystalline lattice [8], the refractive index mappings can have different time durations depending on the type of photorefractive material used [9]: therefore, it is possible to create permanent, semi-permanent or transient waveguides according to the dielectric relaxation of the crystal. For example, bulk crystals of lithium niobate have a very slow dielectric relaxation, so they can be considered almost permanent [6], while the dielectric relaxations of strontium barium niobate [10], indium phosphate [11] and bismuth silicone oxide [12] crystals are relatively fast, therefore inducing transient solitons and solitonic waveguides. In this respect, Diebel et al. [8] demonstrated in strontium barium niobate that photorefractive solitons can be tailored not only through the choice of material, but also by engineering specific quadruple-shaped waveguiding channels capable of implementing all-optical photonic interconnects, illustrating a complementary strategy for functional network architectures based on solitonic structures. Technologically, semi-permanent waveguides are very interesting since they

give rise to sufficiently stable integrated circuits that can be strengthened (for example to implement optical learning techniques [13]) or canceled depending on the experimental needs. The erasing procedure of photorefractive information has been investigated for long time [14, 15]. In general, erasing written structures means eliminating the distribution of the photogenerated charges, for example by re-exciting them optically and then applying an electric field to redistribute them throughout the whole material [16]. J. Petter et al reported that the written solitons are slowly erased by background illumination in strontium barium niobate crystals [17]. Eggert et al [18] used an off-Bragg beam to erase holographic gratings: in this case, the applied electric field was larger than the coercive field of the crystal. Z. Yu et al [19] as well as C. Hou et al [20] show that in two-photon photorefractive media, it is possible to partially erase soliton waveguides by exploiting a single-photon absorption process. E. Fazio et al [1] erased solitonic channels in lithium niobate by homogeneously irradiating the bulk crystals with a laser wavelength within the sensitivity range of the specific material. The authors declare that this procedure requires a duration of 80 minutes, during which it was not possible to carry out further experiments. Interestingly, D. Trader et al report the possibility of erasing the refractive index modulation by applying a strong white light illumination to the crystal [21]. The entire procedure is not described, but the authors report that they were able to make vanish the waveguiding properties and therefore to a broad diffracted Gaussian beam at the crystal output face.

Recently, we have published [22] the formation of solitonic channels within 8-micron thick LNOI films, investigating their properties as X-Junction neurons. In this paper we describe a novel procedure for their in-situ complete erasing.

Methods and Results

The solitonic X-junction writing [22] in LNOI film took advantage of the application of the electric bias through the pyroelectric field. By increasing the crystal temperature of a gradient ΔT, a change of the dipole moment occurs and therefore the spontaneous polarization P decreases due to the pyroelectric effect. As a consequence, a homogeneous pyroelectric field occurs along the c-axis:

$$E_{py} = -\frac{P_y}{\varepsilon}\Delta T \qquad (1)$$

where ε is the static dielectric constant and P_y the pyroelectric coefficient. When ΔT is about 20 °C the E_{py} is 40 kV/cm.

To write the solitonic X-junction we use the same apparatus already described in [22] and reported in Fig. 1. The LNF (Lithium Niobate Film) samples were produced using 500 µm thick, z-cut undoped lithium niobate ($LiNbO_3$) wafers. To begin, a 1 µm silica buffer layer is deposited onto one side of the wafer, followed by a 200 nm sputtered gold layer. An identical gold coating is also applied to a highly flat silicon wafer, and the two surfaces are then pressed together to form a robust gold-to-gold bond. In the final stage, the resulting structure is ground and polished until the lithium niobate layer is reduced to a thickness of 8 µm, creating a slab waveguide integrated onto the silicon substrate with silica and gold intermediate layers.

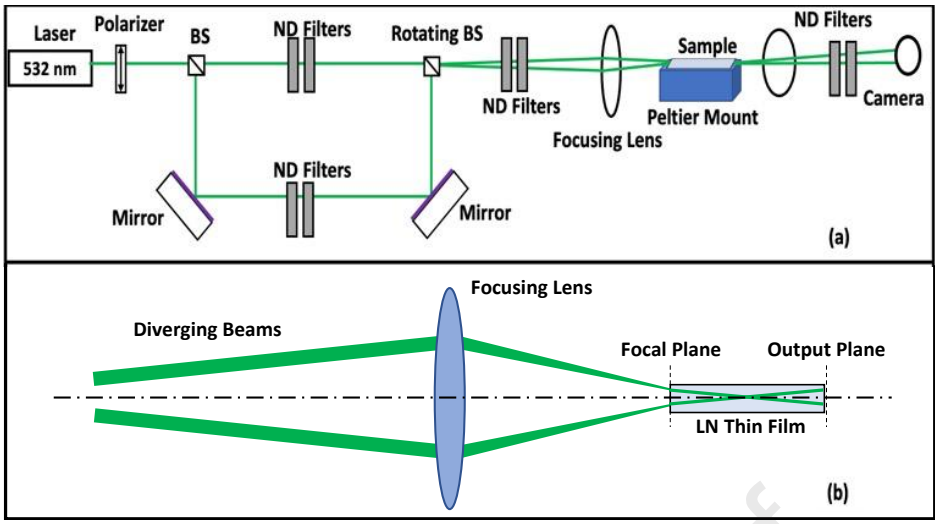

Fig. 1: Experimental set-up for the formation of X-junctions (a) and detailed top view of the two beams trajectory before and inside the slab $LiNbO_3$ waveguide (b).

We injected two incoherent beams at 532 nm inside the LNOI thin planar film. The beams had a small relative angle in order to cross one-each-other at the centre of the sample. In fig.2a you can see the diffracting beams at the output face of the sample: being in a film, beams diffract only in one dimension. In fig.2b the beam self-confinement is shown. Once built, these structures remain stable for long time. E. Fazio et al [1] report the presence of stable solitonic waveguides after months from their writing.

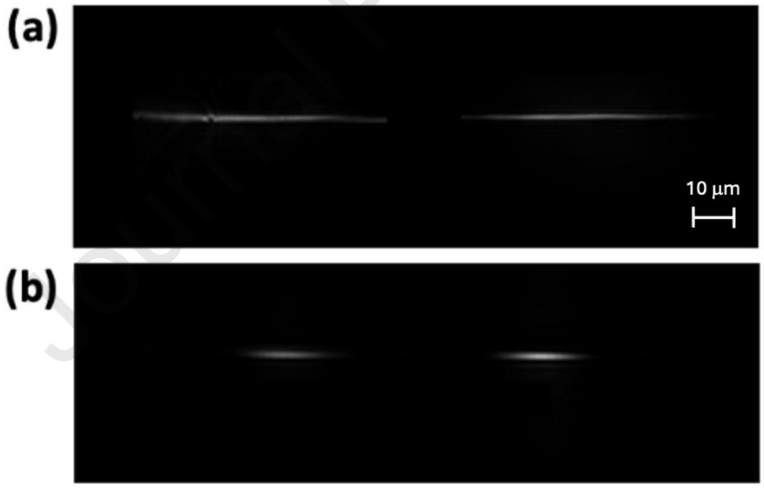

Fig. 2 Writing sequence of an unbalanced X-junction, with higher index contrast towards the left channel. The required time to build the solitons is about 2 minutes with a power of about 10-15 μW. The process takes longer to clear a written channel with higher input power. Scale bar: 10 μm (applies to both panels).

An inconvenient and ineffective procedure was previously carried out to erase. The crystal was placed near a heating white light source and left to be irradiated for hours to days, depending on how deep the index changes had been. This procedure presents two orders of problems: it requires very long action times and it is not local. The irradiation method using a hot light source acts on the whole crystal without distinction: it is not possible to weaken the index contrast for single waveguides or single points. A novel protocol was then implemented to erase the structures. After writing, the laser beams were turned off and the crystal temperature allowed to return to room one ($\Delta T = 0$). This operation cancelled the thermal gradient necessary for the pyroelectric bias field. At this point, the laser beam is reactivated, exactly at the same position as before, with powers of about 80 times larger (about 800 μW for the reported results). Typical writing powers were of the order of 10 μW (with associated formation times of the order of few minutes), while erasing

powers were as high as few mW. Although the high-power erasure beams may induce a localised thermal rise in the crystal, we argue that a thermally-driven pyroelectric contribution to the erasure is negligible. The 8 μm LNOI film is bonded to a silicon substrate (thermal conductivity ~150 W/m·K), which acts as an efficient heat sink; a point-source thermal estimate yields a localised temperature rise well below a few degrees Celsius, far below the $\Delta T \approx 20$ °C required to generate a significant pyroelectric field. More fundamentally, a pyroelectric field acting along the c-axis would be spatially uniform and would not discriminate between channels of different refractive index contrast. The observed difference in erasing time constants between the two arms of the unbalanced X-junction ($\tau \sim 3.33$ s vs $\tau \sim 1.32$ s, for higher and lower refractive index contrasts, respectively) is instead fully consistent with a photovoltaic mechanism, which acts locally where the trapped charge density is highest and therefore produces channel-dependent erasing dynamics.

Such powers excite hot densities of free charges that move around in the crystal, erasing any local distributions and re-homogenizing the whole material. The experimental evolution of the high-intensity erasing beams is shown in figure 3. Initially, fig. 3 (a), the two beams of the X-junction are still confined, but the excited charges start to move in the substrate. As a consequence, fig. 3 (b)-(f), the confine light starts diffracting more and more. Frames were taken every 10 seconds since the erasing times were turned on in order to characterize the whole process evolution. Often, this re-excitation process is inefficient because the excited levels are not simply connected to the others through single-photon transition. The greater the intensity of writing, the more profound states are excited which cannot be completely emptied [23-28]. We observe that this does not happen in thin films: in our case, we managed to completely erase many times the solitonic channels of an X-Junction made in an 8 mm thick film of lithium niobate on insulator [22]. We hypothesize that deep states are influenced by surface defects and that in films they are fewer in number than those present in bulk, with more limited access. The presence of many charges on the edges of the crystals and therefore on surface states makes it more mobile and difficult to trap in deep states. We are carrying out further and specific studies to verify this hypothesis.

In the cancellation process, a fundamental role is played by the photovoltaic field self-generated by the lighting, whose growth and local action are more intense where the distribution of trapped charge is more intense and therefore where a more effective action is necessary to remove it. This is the expedient that makes the procedure here proposed more effective: acting locally, where it is most needed, with a dedicated electric field (the photovoltaic one) to extract the charge and re-mobilize it.

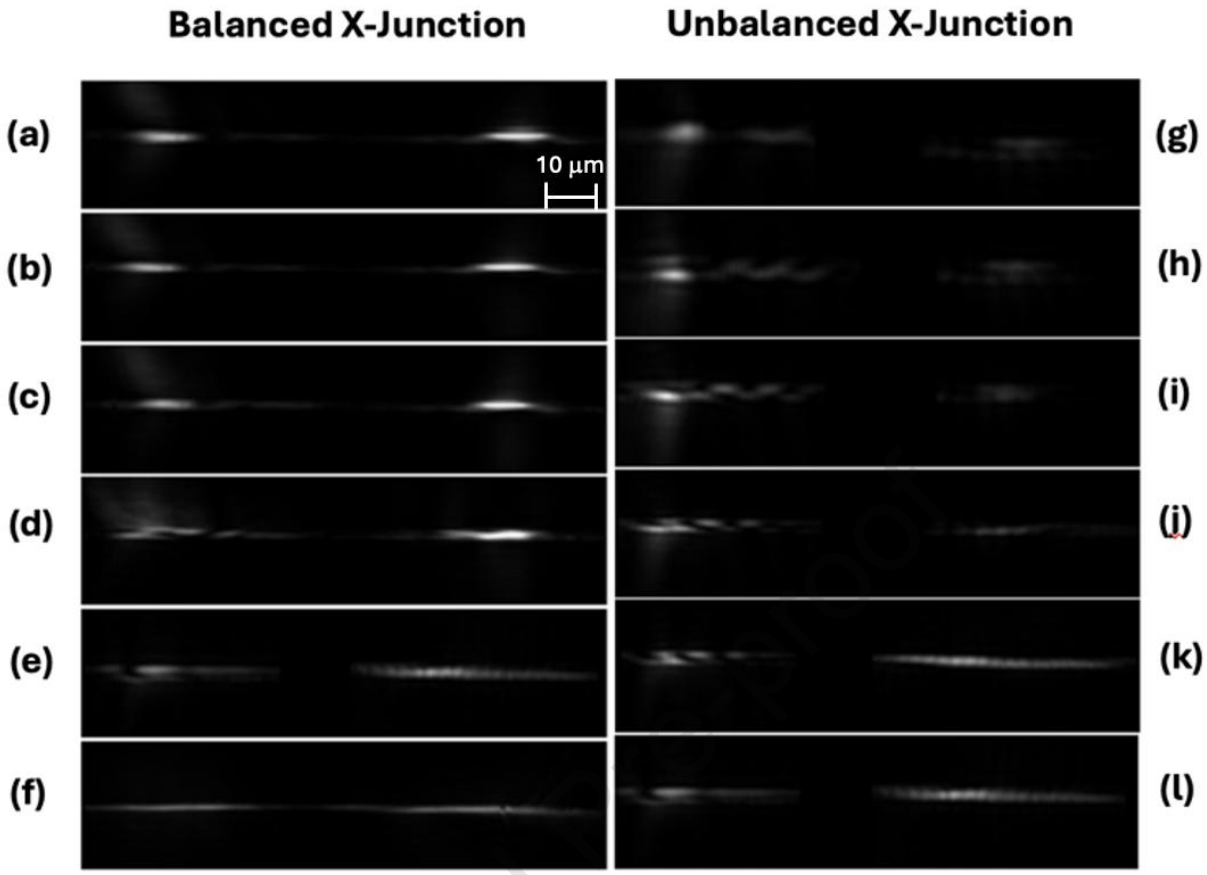

Fig. 3. *From (a) to (f): Erasing sequence of a balanced X-junction. From (g) to (l): Erasing sequence of an unbalanced X-Junction with higher index contrast towards the left channel. Scale bar: 10 µm (applies to all panels).*

This process seems to be affective for any kind of photorefractive distribution: in fig. 3 we also report the erasing dynamics of an unbalanced X-junction too, i.e. a solitonic X-junction with arms of different refractive index contrast. Also in this case, from the initial self-confined state (fig. 3g), the propagating light slowly erases the local charge-distribution making itself diffracts.

Due to the different light intensities inside the unbalanced junction, the cancellation speeds are different for the 2 channels and above all the two arms follow different dynamics that pass through highly inhomogeneous local states (figs. 3 h-k) until the charge is redistributed homogenously and the diffraction of the assumes again a clean and uniform shape (fig. 3 l).

The procedure just described was successfully operated for many successive attempts of both balanced and unbalanced X-junctions. This means that the cancellation was repeated after each writing procedure, always arriving at the same profile, without any kind of photorefractive efficiency degradation. This first result is not exhaustive of the property: we are currently observing whether there are limits in terms of successive times with which the initial conditions can be recovered, or whether there is a progressive slowing down of the winding movement as the number of iterations grows. The erasing dynamics was numerically investigated through simulations with COMSOL Multiphysics software. To address this point, we have clarified in the manuscript the parameters used in the numerical simulations and their correspondence with the experimental conditions. The COMSOL simulations were designed to closely mirror the experimental procedure. In particular, the writing phase was simulated from t = 0 s to t = 120 s, corresponding to the formation of the solitonic channels under writing powers of the order of 10 µW. The stabilization phase was simulated from t = 120 s to t = 160 s, during which both illumination and pyroelectric bias were turned off,

allowing charge redistribution without external driving forces. Finally, the erasing phase was simulated from t = 160 s to t = 280 s, during which high-power beams (up to ~800 μW.) were applied to induce charge re-mobilization and erasure of the refractive index modulation. The entire simulation was performed with a temporal step of 2.5 s, matching the experimental acquisition rate and allowing a direct quantitative comparison between numerical and experimental erasing dynamics. The classical numerical model of photorefractivity [29,30] assumes that donors (and acceptors) reside in fixed trap states, while, conversely, electrons exhibit mobility within the conduction band.

The electron (N_e) generation rate coincides with the generation of ionized donor states (N_D^+) through the equations:

$$\frac{\partial N_D^+}{\partial t} = \sigma F N_D - \gamma N_e (N_A + N_D^+) \qquad (2)$$

$$\frac{\partial N_e}{\partial t} = \frac{\partial N_D^+}{\partial t} + \frac{1}{q}\vec{\nabla}\cdot\vec{J} \qquad (3)$$

with the only difference connected to their mobility, combination of diffusion and conduction. Here $\vec{J}$ represents the current density that is the combination of diffusion, conduction and photovoltaic effect:

$$\vec{J} = \mu k T \vec{\nabla} N_e + q\mu N_e \vec{E} + \beta_{PH}\left[\vec{\nabla}(N_d - N_D^+)I\right]. \qquad (4)$$

The effective electric field present in the lithium niobate film results in the overlapping of the applied bias, the photovoltaic field and the local charge-induced screening field:

$$\vec{E} = \vec{E}_{py} + \vec{E}_{PH} + \frac{\vec{D}_{SC}}{\varepsilon_{PR}} \qquad (5)$$

which is generated, through the Gauss theorem, by the local charge distribution ρ:

$$\rho = q(N_D^+ + N_A - N_e) \qquad (6)$$

being N_A the acceptor density distribution. The electric field (eq.(5)) is the one responsible for both the refractive index distribution writing and erasing. The study is divided into three phases: 1) channel writing (from diffraction to the soliton formation); 2) thermal stabilization, i.e. the thermalization process without thermal gradient and light off; 3) laser reactivation at higher power without external electric bias. Fig. 4 (A) shows the sample geometry as well as the evolution of the refractive index mapping within the thin film of LNOI in the x-z plane. Fig. 4 (B) shows the equivalent excited donor distribution while Fig. 4(C) the corresponding electron distribution.

The values of all parameters used in the COMSOL Multiphysics simulations are listed in Table 1. The material parameters are taken from the literature for congruent undoped $LiNbO_3$ at room temperature; the optical and simulation parameters reflect the experimental conditions described above.

Symbol	Description	Value	Units
σ	Photo-ionisation cross-section [Eq. (2)]	2.0×10^{-17}	$m^2\ J^{-1}$

Symbol	Description	Value	Units
F	Photon flux (writing / erasing) [Eq. (2)]	2.7×10^{17} / 2.1×10^{19}	$m^{-2}\ s^{-1}$
γ	Recombination coefficient [Eq. (2)]	1.0×10^{-12}	$m^{3}\ s^{-1}$
N_D	Total donor density [Eqs. (2), (4)]	1.0×10^{23}	m^{-3}
N_A	Acceptor (trap) density [Eqs. (2), (6)]	1.0×10^{22}	m^{-3}
q	Elementary charge [Eqs. (3), (6)]	1.602×10^{-19}	C
μ	Electron mobility [Eq. (4)]	7.0×10^{-6}	$m^{2}\ V^{-1}\ s^{-1}$
β_{PH}	Photovoltaic coefficient [Eq. (4)]	2.5×10^{-9}	$A\ V^{-1}\ m^{-1}$
$\varepsilon \equiv \varepsilon_{PR}$	Relative permittivity (extraordinary, c-axis) [Eqs. (1), (5)]	28	–
P_y	Pyroelectric coefficient [Eq. (1)]	-4.0×10^{-5}	$C\ m^{-2}\ K^{-1}$
ΔT	Temperature gradient (writing phase; 0 during erasing) [Eq. (1)]	20 / 0	°C
Δt	Simulation time step	2.5	s

Table 1. Input parameters of the COMSOL Multiphysics simulations. All symbols are consistent with Eqs. (1)–(6). Material parameters (σ, γ, N_D, N_A, μ, $\varepsilon \equiv \varepsilon_{p}o$, $\beta_{p}H$, P:⊐) for congruent undoped $LiNbO_3$ are taken from Refs. [29,30]. The photon flux F is derived from the experimental beam powers and the beam cross-section in the 8 μm film. $\Delta T = 0$ during the erasing phase (thermal gradient removed). Variables computed self-consistently by the solver (N_D^+, N_e, J, E, E_pH, D_sc, ρ) are not listed.

After 2.5s from turning on, the propagating light starts generating charges, both trapped (Fig.4 A-a) and free electrons (Fig.4 (C-a)). Consequently, the local electric field associated modifies the refractive index (Fig. 4 A-a). After a sufficient long time (t=120s), the formation of the solitonic channel is almost completed (Fig.4 A-b). A stable distribution of excited donors (Fig. 4 B-b) and a stable distribution of electrons (Fig. 4 C-b) induce a local modification of the refractive index (Fig. 4 A-b) which is able to support a self-confined light beam.
In the stabilization phase, without electric bias and illumination, so the electrons are free to diffuse (Fig. 4 C-c) somehow partially restoring the excited donors (Fig. 4 B-c). However, the whole erasing is possible only after the high-intensity light is turned on, which increases the charges moving (Fig. 4 B-d and 4 C-d) also through the local photovoltaic field which pushes them to reoccupy all available sites. As a consequence, the refractive index mapping thins out becoming almost coincident with the top face of the film, interfaced with the air. This allows the previously written index mapping to be progressively lost until it returns to the diffraction regime condition (Fig. 4 A-d).

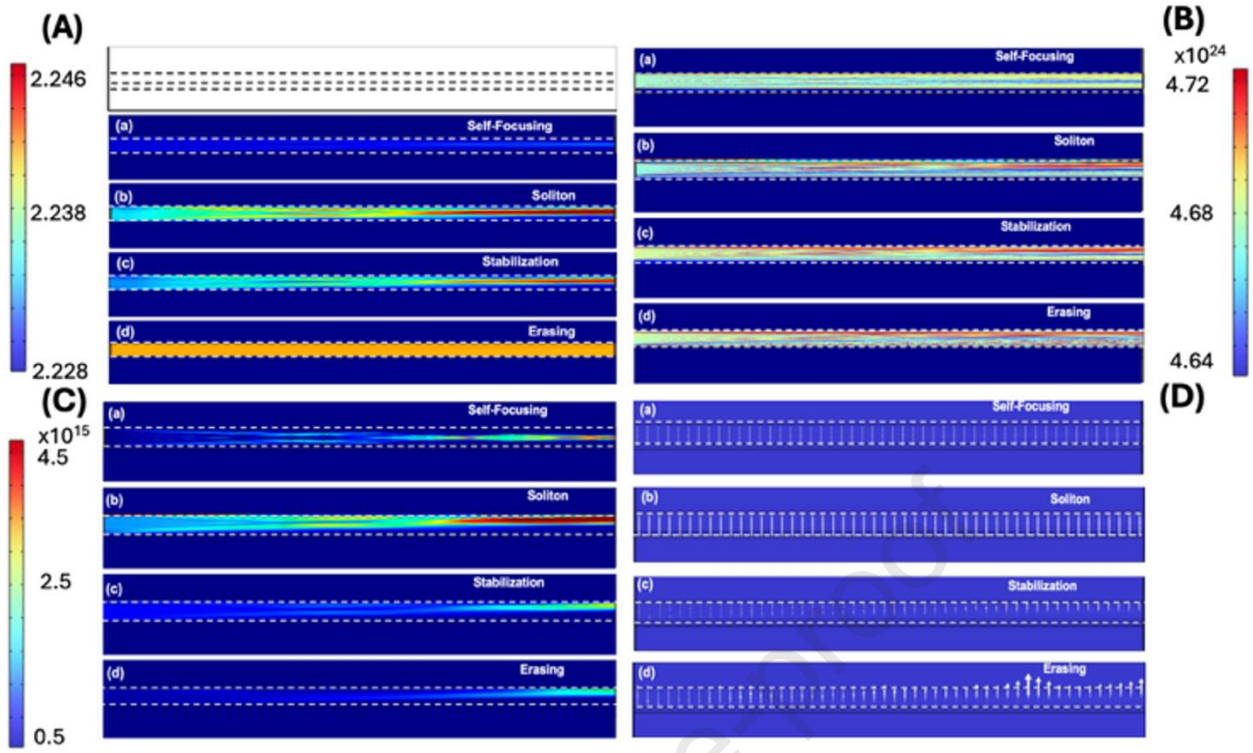

Fig. 4. *Numerical evolution of the photorefractive quantities during the different phases of the process. (A) Refractive index distribution, (B) excited donor density, (C) free-electron density, and (D) total electric field at representative times corresponding to (a) diffraction regime (t = 2.5 s), (b) self-confinement (t = 100 s), (c) stabilization (t = 120 s), and (d) erasing phase (t = 280 s).*

To characterize the erasing efficiency of this method, we analyze the temporal evolution of the output beam profiles during the erasing process for both a balanced X-junction (Fig. 5) and an unbalanced X-junction (Fig. 6). From these measurements, the two-spot beam waist is extracted as a function of time, as shown in Fig.5b for the balanced configuration and in Figs. 6b–c for the unbalanced one. By fitting data with an error function (reported in eq.(7)), we found a time relaxation constant t~1.28s for the two channels in the balanced X-Junction. In the unbalanced structure, the erasing speed is different for the two channels: the channel with higher refractive index contrast showed a time relaxation constant t~3.33s while the one with lower refractive index contrast has a value of t~1.32s.

$$W(t) = W_{sol} + \left(W_{diff} - W_{sol}\right)\frac{1}{2}\left[1 + \mathrm{erf}\left(\frac{t-t_0}{\tau}\right)\right] \qquad (7)$$

In eq. (7), where W_{sol} and W_{diff} are the beam waist in the solitonic and fully diffracted regimes, respectively, t_o is the onset time of the erasing process, and τ is the relaxation time constant.

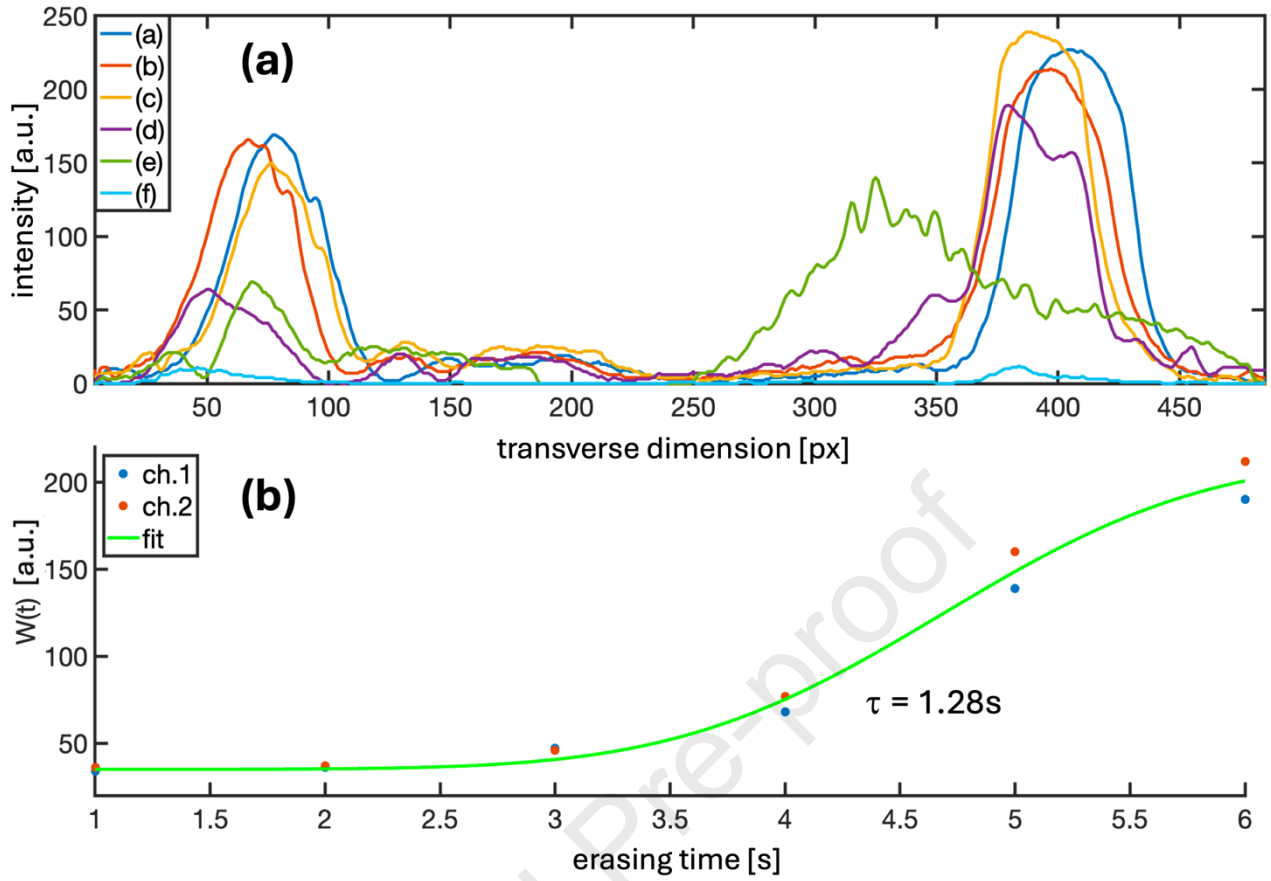

Fig. 5. *(a): Evolution of beams output profile during the erasing procedure in the balanced X-Junction; (b): beam waist evolution as a function of time, the two channels show a time relaxation constant of t~1.28 in the balanced X-Junction.*

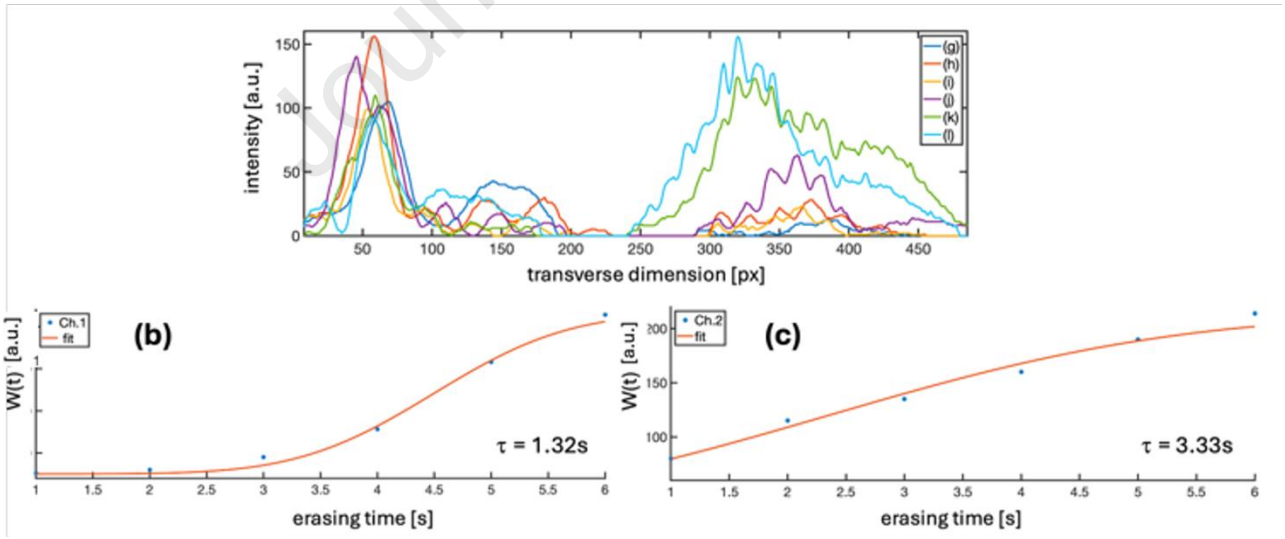

Fig. 6. *(a): Evolution of beams output profile during the erasing procedure in the unbalanced X-Junction; (b): beam waist evolution as a function of time of the channel with lower refractive index contrast. (c): beam waist evolution as a function of time of the channel with higher refractive index contrast.*

To further generalize this result, Fig. 7 reports the characteristic erasing time constant τ as a function of the output splitting ratio of the X-junction. A clear monotonic increase of τ is observed as the splitting ratio increases, indicating that channels associated with higher refractive index contrast require longer erasing times. This behavior confirms that the erasing dynamics are governed by the depth of the photorefractive charge distribution established during the writing process. The observed saturation of τ at high splitting ratios

suggests the onset of a regime limited by charge mobility rather than excitation efficiency, consistently with a diffusion-driven relaxation mechanism.

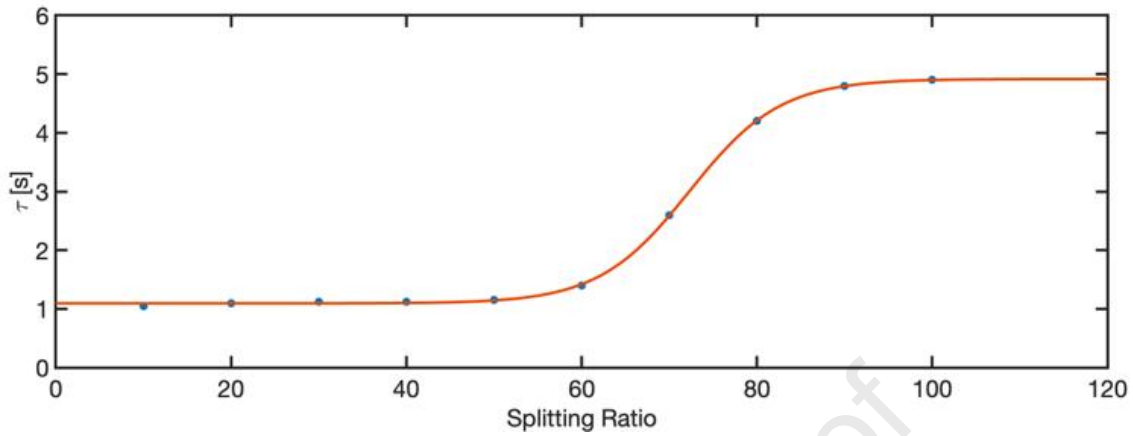

Fig. *7*. Characteristic erasing time constant τ extracted from error-function fits of the beam waist evolution as a function of the output splitting ratio. Higher splitting ratios, corresponding to stronger refractive index modulation, exhibit longer erasing times.

Conclusions

This erasing procedure restores the experimental initial conditions without removing the sample from the writing set-up, which makes the whole process more efficient, letting the light reach all the points where the excited charges are trapped. Such behavior significantly speeded up the erasing procedure too. The advantages of live deletion are also notable from an application point of view. Being able to write and delete information has important application implications in systems capable of learning, that is, where it is essential to record important information and delete less important or superfluous information, such as for example in optical artificial neural networks. Previous work has shown the possibility of learning data by reinforcing the refractive index contrast of solitonic channels.

This work shows that it is also possible to erase information or simply weaken it: compared to previous works for which all photorefractive mapping was eliminated, the protocol developed allows selective erasure of individual channels. The process presented here shows the possibility of intervening locally, on each single solitonic channel, for example to modify the synaptic weight it may have within a complex neural optical network [31]. In neural language, if writing information means learning, erasing the variation of the index therefore becomes synonymous with forgetting, or rather, with creating a new physical space to learn new things.

Funding . Sapienza University of Rome - SEED-PNR call. AMDG. The research and collaboration with the Besançon laboratory were funded with a BGF grant n ° 112590V from the French government. FAZIO-ATENEO_SEED_PNR_2021; FAZIO-ATENEO_PICCOLI_2022; Project PRIN 2022: *ONEPLAST: Optical Neuroplasticity to memorize and recognize information*, granted by EU - NextGenerationEU - CUP B53D23004900006 – Project Code 20222MYZAP PNRR M4.C2.1.1; PNRR-NextGenerationEU, partnership on "Telecommunications of the Future", Grant PE00000001-"RESTART_ELENE". Crowdfunding (GoFundMe) for the Askesis Project.

Disclosures. The authors declare no conflicts of interest.

References

1. M. Segev, B. Crosignani, A. Yariv," Spatial solitons in photorefractive media", et al., Phys. Rev. Lett. 68, 923 (1992)
2. E. Fazio, F.Renzi, R. Rinaldi, et al., "Screening-photovoltaic bright solitons in lithium niobate and associated single-mode waveguides",Appl. Phys. Lett. 85, 2193-2195 (2004).
3. B. Crosignani, G. Salamo, "Photorefractive solitons",Optics & Photonics News 13(2), 38-41 (2002).
4. B. Crosignani, P. Di Porto, M. Segev, et al, Nonlinear optical beam propagation and solitons in photorefractive media. Riv. Nuovo Cim. 21, 1–37 (1998).
5. M. Chauvet, F. Bassignot, F. Henrot, et al., "Fast-beam self-trapping in LiNbO3 films by pyroelectric effect",Opt. Lett. 40, 1258-1261 (2015).
6. Q. Jiang, Y. Su, X. Ji, "Pyroelectric photovoltaic spatial solitons in unbiased photorefractive crystals", Physics Letters A 45, 3085-3087 (2012).
7. Y. Minet, L. Reis, J. Szabados, et al., "Pockels-effect-based adiabatic frequency conversion in ultrahigh-Q microresonators",Opt. Express 28, 2939-2947 (2020).
8. F. Diebel, M. Boguslawski, T. Dadalyan, R. Drampyan, C. Denz, "Controlled soliton formation in tailored Bessel photonic lattices", Opt. Express 24(12), 12933–12940 (2016). doi: 10.1364/OE.24.012933
9. A. Bile, "Solitonic Neural Networks An Innovative Photonic Neural Network Based on Solitonic Interconnections", Springer In (Ed.), AI in Materials –ISBN-10: 3031486544. ISBN-
10. H.Tari, A. Bile, A. Nabizada, et al., "Ultra-broadband interconnection between two SPP nanostrips by a photorefractive soliton waveguide", Opt. Express 31, 26092-26103 (2023).
11. N. Khelfaoui, C. Dan, N. Fressengeas et al., "Fast build up of photorefractive spatial solitons in iron doped indium phosphide", ROMOPTO 2006, 28-31 August 2006, September 2006, Sibiu, Romania.
12. O.V. Kobozev, A. E. Mandel, S. M. Shandarov, et al., Quantum Electron. 30 514 (2000).
13. I. Romdhane and G. Kaddoum, "Nonlinearity of the photorefractive response upon two-beam interaction in a bismuth silicon oxide crystal in an alternating electric field", in IEEE Internet of Things Journal, vol. 9, no. 20, pp. 20270-20281 (2022).
14. Z. Chen, M. Segev, T. H. Coskun, et al., "Coupled photorefractive spatial-soliton pairs", J. Opt. Soc. Am. B 14, 3066-3077 (1997).
15. K.G. Balabaev, V.B. Markov, S.G. Odulov, "Optical erasure of holograms in crystals of lithium niobate", Ukrainian Phys. J. 21(9), 142–146 (1976).
16. G.I. Stegeman, M. Segev, Springer, In: Zakharov, V.E., Wabnitz, S. (eds) Optical Solitons: Theoretical Challenges and Industrial Perspectives. Centre de Physique des Houches, vol 12. (1999).
17. J. Petter, C. Weilnau, C. Denz, et al., "Self-bending of photorefractive solitons", Optics Communications 170, 291-297 (1999).
18. H. A. Eggert, F. Y. Kuhnert, K. Buse, et al., "Trapping of dielectric particles with light-induced space-charge fields", Appl. Phys. Lett. 90, 241909 (2007).
19. Z. Yu et al., Chinese Physics, "Photorefractive soliton interactions in photonic lattices", Chinese Phys. 16, 2149-2154 (2007).
20. C. Hou, Y. Zhang, Y. Jiang, et al.," Photovoltaic solitons in two-photon photorefractive materials under open-circuit conditions", Optics Communications 273, 544-548 (2007).
21. D. Trager, N. Sagemerten and C. Denz, "Guiding of dynamically modulated signals in arrays of photorefractive spatial solitons", IEEE Journal of Selected Topics in Quantum Electronics 12, 383-387 (2006).
22. A. Bile, M. Chauvet, H. Tari et al., "Supervised learning of soliton X-junctions in lithium niobate films on insulator", Optics Letters 47, 5893-5896 (2022).
23. L. Tsarukyan, A. Badalyan, R. Drampyan, "Bending optical soliton-induced waveguide channels in a photorefractive LiNbO3 crystal", Appl. Phys. B 128, 146 (2022).

24. Y. Tan, F. Chen, M. Stepić, et al., “Reconfigurable optical channel waveguides in lithium niobate crystals produced by combination of low-dose O3+ ion implantation and selective white light illumination”, Opt. Express 16, 10465-10470 (2008).
25. M. Bodnar, P. Hribek, “Photovoltaic effect and generation of dark photovoltaic solitons in Fe:LiNbO3”, Proc. SPIE 5949, Nonlinear Optics Applications, (2005).
26. S. Konar, A. Biswas, “Properties of optical spatial solitons in photorefractive crystals with special emphasis to two-photon photorefractive nonlinearity”, Optical Materials, 35, 2581-2603 (2013).
27. Z. Lin, Z. Kang, P. Xu, et al., “Turnkey generation of Kerr soliton microcombs on thin-film lithium niobate on insulator microresonators powered by the photorefractive effect”, Optics Express 29, 42932-42944 (2021).
28. M.Yu, Y. Okawachi, R. Cheng, et al., “Raman lasing and soliton mode-locking in lithium niobate microresonators”Light Sci Appl 9, 9 (2020).
29. A. Zozulya and D. Anderson, “Nonstationary self-focusing in photorefractive media”, Opt. Lett. 20, 837 (1995).
30. A. Zozulya and D. Z. Anderson,” Propagation of an optical beam in a photorefractive medium in the presence of a photogalvanic nonlinearity or an externally applied electric field”, Phys. Rev. A 51, 1520 (1995).
31. A. Bile, H. Tari, E. Fazio, “Episodic memory and information recognition using solitonic neural networks based on photorefractive plasticity”, Appl. Sci., 12, 5585 (2022).

Declaration of interests

☒ The authors declare that they have no known competing financial interests or personal relationships that could have appeared to influence the work reported in this paper.

☐ The authors declare the following financial interests/personal relationships which may be considered as potential competing interests: